Rev. Roum. Sci. Techn.– Électrotechn. et Énerg.
Vol. **62**, *4*, pp. 358–364, Bucarest, 2017

COMPARATIVE STUDY BETWEEN TWO SENSORLESS METHODS FOR DIRECT POWER CONTROL OF DOUBLY FED INDUCTION GENERATOR

ALI IZANLO[1], S. ASGHAR GHOLAMIAN[2], MOHAMMAD VERIJ KAZEMI[3]

Key words: Doubly fed induction generator (DFIG), Direct power control (DPC), Unbalanced voltage, Rotor position estimation.

In this paper two control system proposed and then applied for a DFIG by variable speed wind turbine under unbalanced grid voltage. In this control system the rotor position sensor is eliminated by using two methods for detecting the rotor position. Also, presents an analysis and comparison study of two sensorless methods for the detection of rotor position of the doubly fed induction generator (DFIG). These two methods were compared with each other under different condition *i.e.* various unbalanced voltage, super-synchronous, sub-synchronous and variable speed and in the end, Advantage of any of the methods is expressed. The two methods studied in this paper for rotor position estimation, are rotor current model reference adaptive system (MRAS) and using of a sensorless strategy. Both methods obtained required information for rotor position estimation by measuring stator voltage, stator and rotor current. Till now, has not been used from sensorless algorithms and MRAS observer for DFIGs control when the network voltage is unbalanced. Also, during network unbalance, three selectable control targets are identified for the rotor side converter (RSC), *i.e.* obtaining sinusoidal and symmetrical stator currents, mitigation of active and reactive powers ripples and the cancellation of electromagnetic torque oscillations. A case study on a typical 2 MW DFIG based wind turbine demonstrating the effectiveness of the proposed control methods is verified with simulations in Matlab/Simulink.

1. INTRODUCTION

The DFIG control comprises both the RSC and grid side converter (GSC) controllers so that the RSC controls stator active and reactive powers and the GSC regulates dc link voltages as well as generation an independent reactive power that is injected into the grid. The DFIG can be controlled by well-known field oriented control (FOC) [1], direct torque control (DTC) [2] or direct power control (DPC). During the recent period, the DPC strategies have also been development to control DFIG systems [3–7].

A simple position sensorless method for rotor side field oriented control of a wound rotor induction machine is described in [8]. The algorithm is based on axis transformation. Compared to the other methods, it is more direct and the dependence on machine parameters is also largely reduced. In [9], the previous sensorless idea using for DPC of a single voltage source converter (VSC) based DFIG. In [10] presents a stator flux based MRAS structure for observing the rotor position and speed of a DFIM.

More recently, the application of DPC for the DFIG under unbalanced grid voltage condition has also been reported [11–14]. Basically, the available unbalanced control methods were based on the symmetrical component theory, which states that an unbalanced system is a combination of the positive and negative networks. In [11] a new kind of reference power generation technique for DPC were proposed to eliminate the torque and power pulsations. It was shown that the oscillation term of electromagnetic torque can be eliminated without any sequence extraction. Izanlo *et al.* [12] proposed a new DPC method under transient unbalanced grid voltage. He used from a new converter in rotor and grid side and presented a new switching table for them. In [13, 14] an model predictive direct power control with power compensation and three selective control targets presented, obtaining sinusoidal and symmetrical grid current, removing active and reactive power ripples and mitigation torque oscillation, in order to enhance the control flexibility and performance of the DFIGs when the network is unbalanced.

2. DYNAMIC BEHAVIOUR OF A DFIG IN THE STATOR STATIONARY FRAME

The mathematical equations for a DFIG can be expressed in the stationary frame (αβ frame) using complex vectors. These are now well known but for completeness they are quoted below [3]

$$V^s_{s\alpha\beta} = R_s I^s_{s\alpha\beta} + \dot{\psi}^s_{s\alpha\beta} \tag{1}$$

$$V^s_{r\alpha\beta} = R_r I^s_{r\alpha\beta} + \dot{\psi}^s_{r\alpha\beta} - j\omega_r \psi^s_{r\alpha\beta} \tag{2}$$

$$\psi^s_{s\alpha\beta} = L_s I^s_{s\alpha\beta} + L_m I^s_{r\alpha\beta} \tag{3}$$

$$\psi^s_{r\alpha\beta} = L_m I^s_{s\alpha\beta} + L_r I^s_{r\alpha\beta} \tag{4}$$

$$P_s = \frac{3}{2}\mathrm{Re}\left\{V_s . I^*_s\right\} = \frac{3}{2}\left\{V^s_{s\alpha} I^s_{s\alpha} + V^s_{s\beta} I^s_{s\beta}\right\} \tag{5}$$

$$Q_s = \frac{3}{2}\mathrm{Im}\left\{V_s . I^*_s\right\} = \frac{3}{2}\left\{V^s_{s\beta} I^s_{s\alpha} - V^s_{s\alpha} I^s_{s\beta}\right\} \tag{6}$$

$$T_e = \frac{3}{2} p\,\mathrm{Im}\left\{\psi^*_s . I_s\right\} = \frac{3}{2} p\left\{\psi^s_{s\alpha} I^s_{s\beta} - \psi^s_{s\beta} I^s_{s\alpha}\right\}, \tag{7}$$

where the phasors and variables are define as

P_s, Q_s	– Stator active and reactive powers;
P_{const}, Q_{const}	– Stator original power references;
P_1, P_2, P_3, P_4	– Active power components;
Q_1, Q_2, Q_3, Q_4	– Reactive power components;
V_s, V_r	– Stator and rotor voltage vectors;
I_s, I_r	– Stator and rotor current vectors;
R_s, R_r	– Stator and rotor resistance;
$L_{\sigma s}$, $L_{\sigma r}$	– Stator and rotor leakage inductance;

[1] izanlo_ali@yahoo.com
[2] Babol Noshirvani University of Technology, Babol, Iran, sagholamian@gmail.com (*Corresponding Author*)
[3] mohammad_v_kazemi@yahoo.com

L_m – Magnetizing inductance;
ψ_s, ψ_r – Stator and rotor flux vectors;
T_e – Electromagnetic torque;
ω_r, ω_s, ω_m – Rotor, stator and slip speeds;
p – Number of pole pairs;
* – Donates the complex conjugate operation.

3. POWER COMPENSATION STRATEGIES UNDER UNBALANCED CONDITION

In this section, the control strategies that injection sinusoidal and symmetric stator current into the grid, and produces constant active and reactive power and electromagnetic torque will be analyzed.

In unbalanced condition stator active and reactive powers and electromagnetic torque by forgoing from the stator resistance can be written as [12]

$$P_s = \frac{3}{2}(P_1 + P_2 + P_3 + P_4) \tag{8}$$

$$Q_s = \frac{3}{2}(Q_1 + Q_2 + Q_3 + Q_4) \tag{9}$$

$$T_e = \frac{3p}{2\omega_s}(P_1 - P_2 + P_3 - P_4). \tag{10}$$

The pulsation terms P_1, Q_1 and P_2, Q_2 are constant at steady state, because they are composed by the same sequence product. However, terms P_3, Q_3 and P_4, Q_4 oscillate at twice the grid frequency pulsation, since they are composed by positive and negative sequence products.

3.1. ACTIVE AND REACTIVE POWER OSCILLATION CANCELLATION STRATEGY (TARGET 1)

In order to obtain constant active and reactive power, the both of them reference must be kept constant, thus the active and reactive power ripples must be zero, *i.e.* [11]

$$P_3 + P_4 = 0 \tag{11}$$

$$Q_3 + Q_4 = 0. \tag{12}$$

As a result, the required powers for compensation become

$$P_{ref} = P_{const} = P_1 + P_2 \tag{13}$$

$$Q_{ref} = Q_{const} = Q_1 + Q_2. \tag{14}$$

According to the (10) and (11), even if the stator active and reactive power pulsation can be removed by the unbalanced DPC, the torque pulsation will still exist.

3.2 TORQUE OSCILLATION CANCELLATION STRATEGY (TARGET 2)

This objectives is to mitigate the torque oscillation when the network is unbalanced. According to (10), the only way to achieve constant electromagnetic torque is by imposing [11]

$$P_3 - P_4 = 0. \tag{15}$$

As a result, the required active power for compensation become

$$P_{ref} = P_{const} + 2P_3 = P_{const} + 2P_4. \tag{16}$$

Since the condition for torque oscillation cancellation in (15) is not related to reactive power, no compensation is needed for the reactive power; that is, $Q_{ref} = 0$.

3.3. SINUSOIDAL AND BALANCED STATOR CURRENT EXCHANGED WITH GRID (TARGET 3)

If P_4 and Q_4 are added to the original power references to obtain the new power references, P_3 and Q_3 can be forced to zero; that is, the negative sequence current is eliminated. In other words, $I_{s\alpha}^-$ and $I_{s\beta}^-$ have to be zero if P_3 and Q_3 are to be maintained as zero.

Therefore, the compensating power pulsations become [13]

$$P_{ref} = P_{const} + P_4 \tag{17}$$

$$Q_{ref} = Q_{const} + Q_4. \tag{18}$$

In the above equation, P_{const} and Q_{const} are equal to original power references under balanced grid voltage condition.

4. IMPLEMENTED SENSORLESS CONTROL METHODS

To increase the reliability of the grid synchronization process, it is important to implement the sensorless rotor position control. There are two main methods that are been used for the detection of rotor position: 1) derived from a shaft sensor, 2) derived from a sensorless algorithm. Sensorless operation is more desirable than using shaft sensor, because the shaft sensor has several disadvantages related to the cost, cabling between the sensor and the controller, robustness and maintenance. The rotor current of DFIGs is available for measurement, which is not possible in cage rotor induction machines. This provides more flexibility in designing sensorless control schemes for DFIGs.

In this study, DPC methods were used to implement the two sensorless control algorithm under unbalanced grid voltage. The DPC of DFIG under unbalanced condition has already been studied before, but there are nothing reports related to the use of sensorless algorithms and MRAS observer for DFIGs control when the network voltage is unbalanced. Figure 1 shows the schematic diagram of the improved control scheme for sensorless DPC of grid connected DFIGs when the network voltage is unbalanced. The proposed compensation methods for powers, torque and stator current oscillation, and too rotor position estimation block, under unbalanced grid voltage conditions shown in Fig. 1. It can be seen from the figure, the compensating powers is calculated according to (13), (14) or (16) or (17), (18), as shown in the dotted line block. A notch filter turned at double grid frequency has been adopted to extract positive and negative sequences stator current and voltage. The filter may involve some amplitude and phase errors that may worsen the control effect. However, since the notch filter is just used to calculate the compensating power and it lies out of the power control loop, the inherent defects caused by sequential decomposition, such as slow dynamic response and low bandwidth of the control loop,

could be avoid. As it is known, performance of the DPC for DFIG depends on the accuracy of rotor position measurement. In Fig. 3, the rotor position is obtained from rotor position detection block and two different sensorless control methods are used inside this block. One of these methods is sensorless algorithm and the other rotor current based MRAS observer.

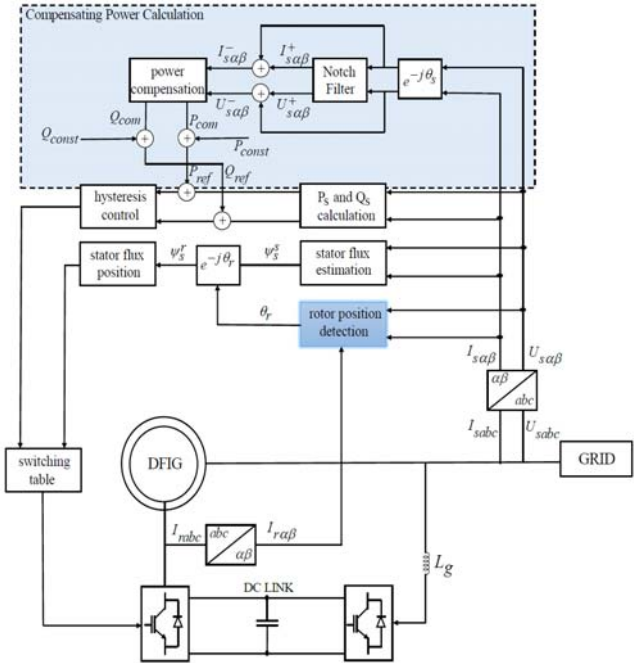

Fig. 1 – The proposed schematic diagram of the sensorless DPC for DFIG under unbalanced condition.

4.1. SENSORLESS ALGORITHM

Seen from the stator coordinate system, (I_r) makes an angle θ_S. Figure 2 shows the same rotor current makes an angle θ_r with the rotor axis. The problem, therefore, is to compute θ_S and θ_r, so that $(\theta_m)_{es} = (\theta_S - \theta_r)$ can be determined.

Rotor current magnitude and unit templates of rotor currents aligned to rotor axis are calculated as [8–9]

$$\left|I_r\right| = \sqrt{I_{r\alpha}^2 + I_{r\beta}^2} \tag{19}$$

$$\cos\theta_r = \frac{I_{r\alpha}^2}{\left|I_r\right|} \quad , \quad \sin\theta_r = \frac{I_{r\beta}^2}{\left|I_r\right|}. \tag{20}$$

The rotor current unit templates ($\cos\theta_s, \sin\theta_s$) aligned to the stator coordinate system has to be calculated. Using previous unit template samples two phase rotor currents ($I_{r\alpha}, I_{r\beta}$) are converted into stator coordinates as

$$I'_{rs\alpha}[k] = I_{r\alpha}[k]*(\cos\theta_m[k-1])_{est} - \\ - I_{r\beta}[k]*(\sin\theta_m[k-1])_{est} \tag{21}$$

$$I'_{rs\beta}[k] = I_{r\alpha}[k]*(\cos\theta_m[k-1])_{est} + \\ + I_{r\beta}[k]*(\sin\theta_m[k-1])_{est}, \tag{22}$$

where k is the present sample, (k-1) is the previous sample, superscript ' indicates the intermediate variable, where $(\cos\theta_m[k-1])_{est}$ and $(\sin\theta_m[k-1])_{est}$ are the unit vectors of rotor position estimated in previous sample.

In terms of the stator and rotor currents, the stator flux magnetizing current (I_{ms}) in stator coordinate system can be expressed as

$$I'_{ms\alpha}[k] = (1+\sigma_s)I_{s\alpha}[k] + I'_{rs\alpha}[k] \tag{23}$$

$$I'_{ms\beta}[k] = (1+\sigma_s)I_{s\beta}[k] + I'_{rs\beta}[k] \tag{24}$$

$$I'_{ms} = \sqrt{I'^2_{ms\alpha} + I'^2_{ms\beta}}, \tag{25}$$

where $\sigma_s = (L_s L_r - L_m^2)/L_s L_r$ is the stator leakage factor.

The stator flux magnetizing current vector (I_{ms}) makes an angle ($\theta - 90$) with the stator axis. Its α, β components can be written as

$$I_{ms\alpha} = I_{ms}\sin\theta \tag{26}$$

$$I_{ms\beta} = -I_{ms}\cos\theta, \tag{27}$$

where

$$\sin\theta = \frac{V_{s\beta}}{\sqrt{V_{s\alpha}^2 + V_{s\beta}^2}} \tag{28}$$

$$\cos\theta = \frac{V_{s\alpha}}{\sqrt{V_{s\alpha}^2 + V_{s\beta}^2}}. \tag{29}$$

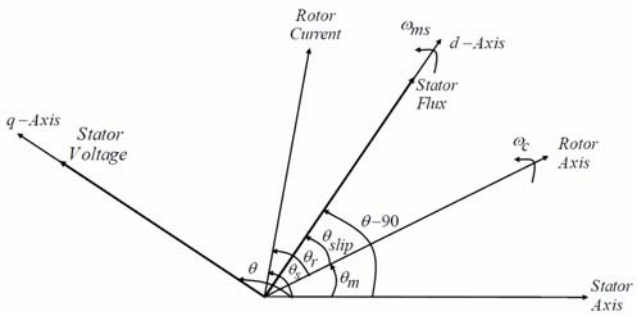

Fig. 2 – Phasor diagram for rotor position estimation sterategy.

Using above I_{ms} and measured value of stator current (I_s), the rotor currents can be computed in the stationary frame as

$$I_{rs\alpha} = I_{ms\alpha} - (1+\sigma_s)I_{s\alpha} \tag{30}$$

$$I_{rs\beta} = I_{ms\beta} - (1+\sigma_s)I_{s\beta} \tag{31}$$

$$\left|I_r^s\right| = \sqrt{I_{rs\alpha}^2 + I_{rs\beta}^2}. \tag{32}$$

The unit vectors of rotor current in stationary coordinate system are given by

$$\sin\theta_s = \frac{I_{rs\beta}}{\left|I_r^s\right|} \quad , \quad \cos\theta_s = \frac{I_{rs\alpha}}{\left|I_r^s\right|}. \tag{33}$$

Equations (20) and (33) represent the unit vectors in the two reference frames, the former rotating at synchronous speed and, the latter at slip frequency. The unit vectors pertaining to the rotor position $(\theta_m)_{est} = (\theta_s - \theta_r)$ can now be easily computed

$$\cos(\theta_m)_{est} = \cos(\theta_s - \theta_r) = \cos(\theta_s)\cos(\theta_r) + \\ + \sin(\theta_s)\sin(\theta_r) \quad (34)$$

$$\sin(\theta_m)_{est} = \sin(\theta_s - \theta_r) = \sin(\theta_s)\cos(\theta_r) - \\ - \cos(\theta_s)\sin(\theta_r) \quad (35)$$

The unit vectors of slip angle are used in below equation for finding the stator flux vector in rotor reference frame. This is equation as

$$\psi_s^r = (\psi_{s\alpha} + j\psi_{s\beta})\{\cos(\theta_m)_{est} - j\sin(\theta_m)_{est}\}, \quad (36)$$

where the stator flux linkages are calculated as

$$\psi_{s\alpha\beta} = \int (V_{s\alpha\beta} - R_s I_{s\alpha\beta})dt. \quad (37)$$

4.2. MRAS OBSERVER

The proposed observer is based on comparison of two signals the first comes from a model reference (MR) block, which is independent from speed value, whereas the second is obtained from adaptive system (AS) which includes speed value. The error signal between MR and AS is applied to adaptation mechanism (AM). The output of the AM is a tuning signal used to adjust the AS for which the error is minimized. Fig. 3 shows a block diagram of an MRAS observer [10].

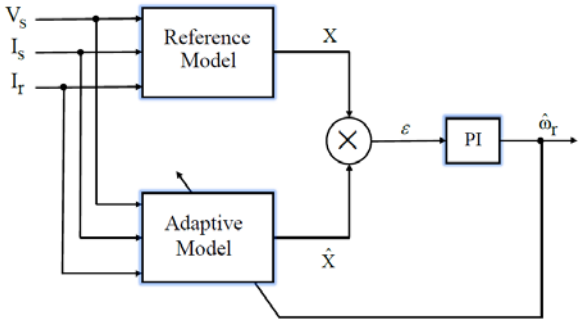

Fig. 3 – Block diagram of a MRAS observer.

From (3), the rotor current is calculated as

$$I_{r\alpha\beta}^s = \frac{\psi_{s\alpha\beta}^s - L_s I_{s\alpha\beta}^s}{L_m}, \quad (38)$$

where $\psi_{s\alpha\beta}^s$ can be calculated based on (37). The error between the measured rotor current and the estimated from (53) can be expressed as

$$\varepsilon = \hat{I}_{r\alpha}^s \times I_{r\beta}^s - I_{r\alpha}^s \times \hat{I}_{r\beta}^s. \quad (39)$$

The error ε in (39) is the cross product between the real and estimated rotor current vectors. This error is driven to zero by a proportional-integral (PI) controller. The implementation of the MRAS observer is shown in Fig. 4. In the practical implementation of (37), a band pass filter is used as a modified integrator to block the dc components of the measured voltages and currents. Since V_s and I_s are at a frequency well above the filter cut-off frequency, there is no deterioration in integral action.

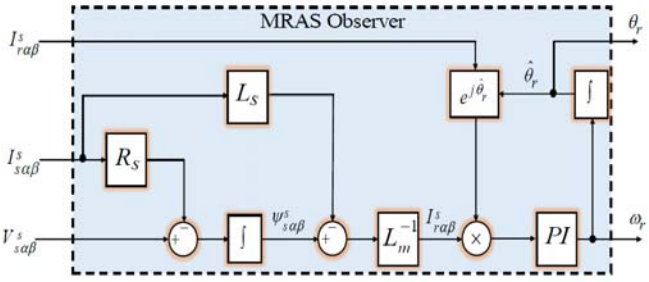

Fig. 4 – MRAS observer structure.

5. SIMULATION RESULTS

The proposed DPC algorithm with two sensorless control methods for DFIG application is designed and simulated in MATLAB/Simulink software. The nominal converter dc link voltage was set at 1 200 V. During simulation, the sampling frequency is 20 kHz and the bandwidths of the active and reactive power hysteresis controllers are set at ±4% of the rated generator power of 2 MW.

The performance of the system will be analyzed under steady-state operation condition. The grid voltages unbalance programmed for this experiment are ($V_{sa} = 0.95 < 0$, $V_{sb} = 0.83 < -113$, $V_{sc} = 0.99 < -210$, yielding 0.91 of positive sequence and 0.09 of negative sequence in per unit (p.u.) value). The DFIG was assumed to be in speed control, *i.e.*, the rotor speed is set externally, as the large inertia of the wind turbine results in slow change of rotor speed. The various stator power references applied, *i.e.*, active and reactive power reference are changed from 1 to –1 (p.u) at 0.16 s and from –0.33 to 0.33 (p.u) at 0.14 s, respectively in different condition (constant speed of 0.8 p.u, constant speed of 1.2 p.u, and 50 % increasing in all inductance), where the synchronous speed was defined as 1 unit.

As shown in the previous section, Target 3 give good attenuations of both torque and active power oscillation. For Target 1, while the active power oscillation is greatly reduced, the torque pulsation is relatively large. Similar observation can also be noticed for Target 2. The selection of the control target is highly dependent on the design of the turbine system and the operation of the network.

In Fig. 5, the Target 1, *i.e.*, active and reactive power oscillation cancellation strategy, was selected as the control objective.

In Fig. 6, the Target 2, *i.e.*, electromagnetic torque oscillation cancellation strategy, was selected as the control objective. The second half, of Fig. 6a shows the power tracking behavior in order to cancel the electromagnetic torque oscillation. Figure 6b shows the current exchanged through the stator under these operation conditions. In the simulation results, a strong deterioration of the currents can be observed before 0.14 s. This fact is due to the oscillating behavior of the electromagnetic torque during this first half of the experiment. In addition, when the torque oscillation cancellation strategy is operating, the stator currents are unbalanced, but sinusoidal.

In Fig. 7, the Target 3 of the power compensation scheme is implemented. As shown in Fig. 7, it can be observed that there are oscillating components in both the active and reactive powers because of the two oscillating terms P_4 and Q_4 added to the original constant active and reactive powers. However, these eliminate the negative sequence current. As a result, the stator current become quite sinusoidal and symmetric, thus power quality is improved significantly.

More tests were accomplished on sensorless DFIG and results placed in Table 1. A comparison between two sensorless methods under different condition was carried out, and each of the methods that have better performance in tracking power reference and lower ripple, introduced. For calculate the active and reactive power ripples we define $\Delta P = \int (P - P_{ref})^2 \mathrm{d}t$ and $\Delta Q = \int (Q - Q_{ref})^2 \mathrm{d}t$ in definite time span. According to the Table, in all conditions MRAS observer method performs better in low voltage unbalance with variable and constant power reference, but the sensorless algorithm method is better in high voltage unbalanced with variable and constant power reference.

Also, both of two ways has good performance to the changes in the *R*s and *L*s parameters. For this reason this tests have not been put in table. It can be noted, the grid low voltage unbalance programmed for this experiment is (*V*sa = 0.73 < 0, *V*sb = 0.7 < –116, *V*sc = 0.79 < –237, yielding 0.74 of positive sequence and 0.04 of negative sequence in per unit (p.u.) value) and the high voltage unbalance is (*V*sa = 0.95 < 0, *V*sb = 0.83 < –113, *V*sc = 0.99 < –210, yielding 0.91 of positive sequence and 0.09 of negative sequence in per unit (p.u.) value). To view more information refer to corresponding table.

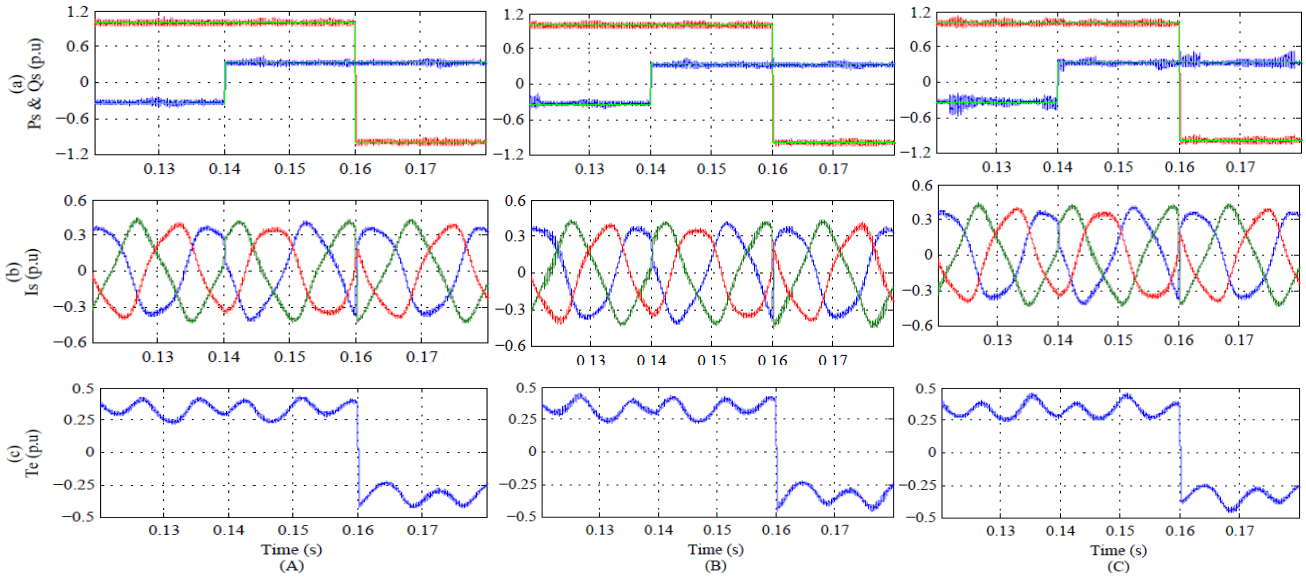

3.1 3.2 3.3

Fig. 5 – Simulation results comparison for positioning the rotor with sensor (3.1), without sensor by using of sensorless strategy (3.2) without sensor by using of MRAS observer (3.3), and with power compensation for target 1 (for rotor speed 0.8 p.u.): a) stator active, and reactive powers (p.u); b) stator currents (p.u); c) electromagnetic torque (p.u).

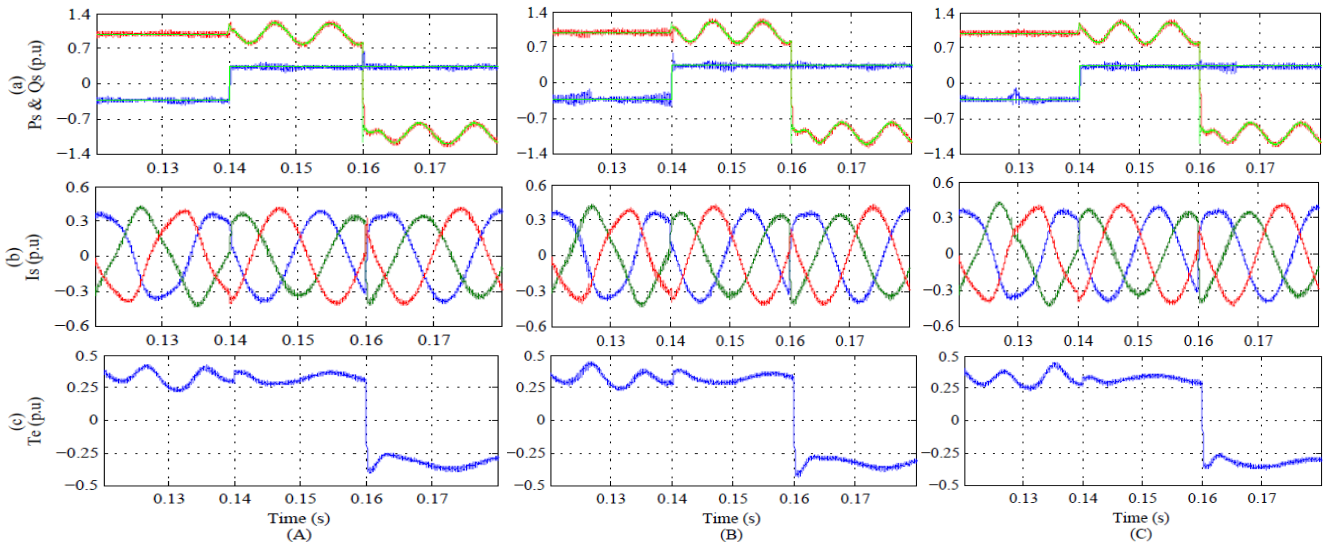

3.1 3.2 3.3

Fig. 6 – Simulation results comparison for positioning the rotor with sensor (3.1), without sensor by using of sensorless strategy (3.2) without sensor by using of MRAS observer (3.3), and with power compensation for target 2 (for rotor speed 1.2 p.u.): a) stator active, and reactive powers (p.u); b) stator currents (p.u); c) electromagnetic torque (p.u).

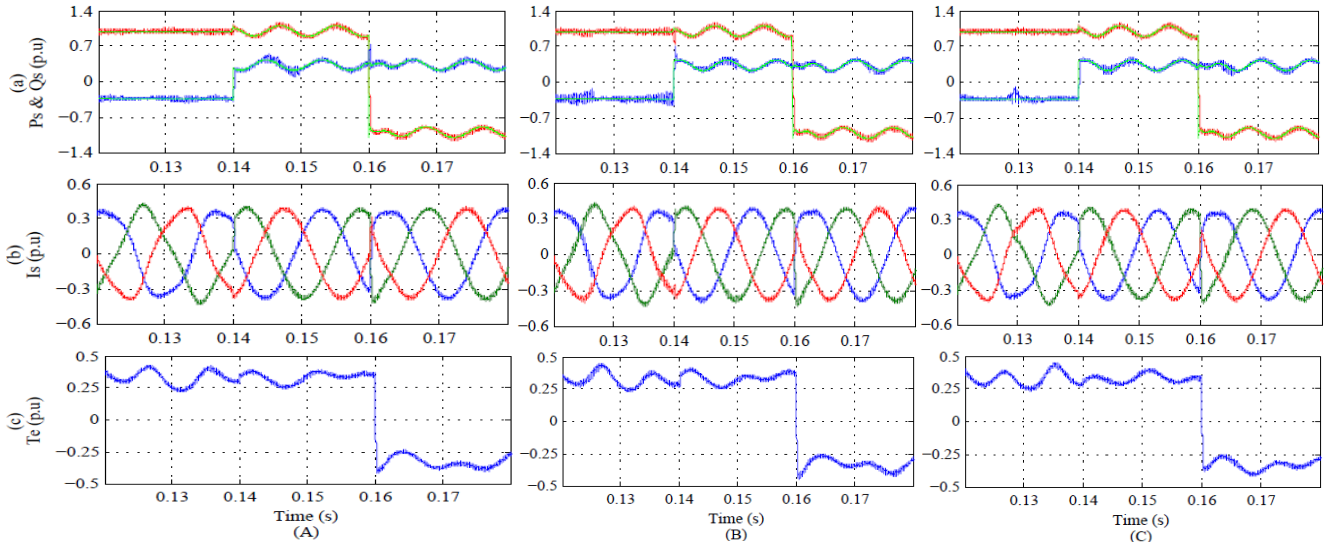

3.1 3.2 3.3

Fig. 7 – Simulation results comparison for positioning the rotor with sensor (3.1), without sensor by using of sensorless strategy (3.2) without sensor by using of MRAS observer (3.3), and with power compensation for target 3 (for 50% increasing all inductances): a) stator active, and reactive powers (p.u); b) stator currents (p.u); c) electromagnetic torque (p.u).

Table 1

Comparison between two sensorless method in different condition

		Low voltage unbalance with variable power reference	Low voltage unbalance with constant power reference	High voltage unbalance with variable power reference	High voltage unbalance with constant power reference
Sub-synchronous speed (0.8 p.u)	Target 1	MRAS observer	MRAS observer	Sensorless algorithm	Sensorless algorithm
	Target 2	MRAS observer	MRAS observer	Sensorless algorithm	Sensorless algorithm
	Target 3	MRAS observer	MRAS observer	Sensorless algorithm	Sensorless algorithm
Super-synchronous Speed (1.2 p.u)	Target 1	MRAS observer	MRAS observer	Sensorless algorithm	Sensorless algorithm
	Target 2	MRAS observer	MRAS observer	Sensorless algorithm	Sensorless algorithm
	Target 3	MRAS observer	MRAS observer	Sensorless algorithm	Sensorless algorithm
Variable Speed (from 1.2 to 0.8 p.u)	Target 1	MRAS observer	MRAS observer	Sensorless algorithm	Sensorless algorithm
	Target 2	MRAS observer	MRAS observer	Sensorless algorithm	Sensorless algorithm
	Target 3	MRAS observer	MRAS observer	Sensorless algorithm	Sensorless algorithm

6. CONCLUSION

This paper presented two control system for DFIG based wind energy generation system operating under unbalanced network condition. Methods for providing enhanced system control and operation for DFIG based wind turbines during network unbalance *i.e.*, power, torque, or stator current oscillation minimization, are identified. This three selectable control targets used for compensating. Simulation confirms the effectiveness and robustness of the proposed DPC strategy during various operating condition. Also, in this paper presented a comparison between two sensorless control techniques under unbalanced network condition: sensorless algorithm and rotor current based MRAS observer. The simulation results shows that the performance of these sensorless methods are similar for operation of DFIG. However, there are some small differences between these methods. In sub synchronous speed, the MRAS observer method is much better. But in super synchronous and variable speed and in high voltage unbalanced the sensorless algorithm method have better performance. In the other words, at low speeds the use of MRAS observer and at variable speeds the use of sensorless algorithm is suitable. Overall, both of these sensorless control methods have acceptable results for operation of DFIG.

Received on July 29, 2016

REFERENCES

1. Fayssal Amrane *et al.*, *Design and Implementation of High Performance Field Oriented Control for Grid Connected Doubly Fed Induction Generator Via Hysteresis Rotor Current Controller*, Rev. Roum. Sci. Techn. – Électrotechn. et Énerg., **61**, *4*, pp. 319–324 (2016).
2. Salah Tamalouzt *et al.*, *Direct Torque Control of Wind Turbine Driven Doubly Fed Induction Generator*, Rev. Roum. Sci. Techn. Électrotechn. et Énerg., **61**, *3*, pp. 244–249 (2016).
3. Lie Xu, Phillip Cartwright, *Direct Active and Reactive Power Control of DFIG for Wind Energy Generation*, IEEE Trans. Energy Conv., **21**, *3*, pp. 750–758 (2006).
4. Dawei Zhi, Lie Xu, Barry W. Williams, *Model-Based Predictive Direct Power Control of Doubly Fed Induction Generators*, IEEE Trans. Power Electron., **25**, *2*, pp. 341–351 (2010).
5. Abdelfettah Kerboua, Mohamed Abid, *Hybrid Fuzzy Sliding Mode Control of a Doubly Fed Induction Generator in Wind Turbins*, Rev. Roum. Sci. Techn. – Électrotechn. et Énerg., **57**, *4*, pp. 412–421 (2012).
6. Nasrin Kalamian, Mohammad Verij Kazemi, S. Asghar Gholamian, *Direct Power Control of DFIG By Using Nonlinear Model Predictive Controller*, Asian Journal of Control, **18**, *4*, pp. 985–999 (2016).
7. M. Adjoudj *et al.*, *Sliding mode control of a doubly fed induction generator for wind turbines, conversion systems*, Rev. Roum. Sci. Techn. – Électrotechn. et Énerg., **56**, *1*, pp. 15–24 (2011).

8. Rajib Datta, V.T. Ranganathan, *A Simple Position Sensorless Algorithm for Rotor Side Field Oriented Control of Wound Rotor Induction machine*, IEEE Trans Ind. Electron., **48**, *4*, pp. 786–793 (2001).
9. Bhim Singh, N.K. Swami Naidu, *Direct Power Control of Single VSC Based DFIG without Rotor Position Sensor*, IEEE Trans. Ind. Applicat., **50**, *6*, pp. 4152–4163 (2014).
10. Roberto Cardenas, Rubem Pena, Jose Proboste, Greg Asher, Jon Clare, *MRAS Observer for sensorless Control of Standalone Doubly Fed Induction Generators*, IEEE Trans Energy Conv., **20**, *4*, pp. 710–718 (2005).
11. Gonzalo Abad, Miguel Angel Rodriguez, Grzegorz Iwanski, Javier Poza, *Direct Power Control of Douby-Fed-Induction-Generator-Based Wind Turbine Under Unbalanced Grid Voltage*, IEEE Trans Power Electron., **25**, *2*, pp. 442–452 (2010).
12. Ali Izanlo, Asghar Gholamian, Mohammad Verij Kazemi, *A New DPC Method For Single VSC Based DFIG Under Unbalanced Grid Voltage Condition*, IEEE Power Electronic, Drive Systems & Technologies Conference 2016, pp. 348–353.
13. Jiefeng Hu, Jianguo Zhu, David G. Dorrell, *Predictive Direct Power Control of Doubly Fed Induction Generators Under Unbalanced Grid Voltage Conditions for Power Quality Improvment*, IEEE Trans Sustain. Energy, **6**, *3*, pp. 943–950 (2015).
14. Jiefeng Hu, Jianguo Zhu, David G. Dorrell, *Model-Predictive Direct Power Control of Doubly Fed Induction Generators Under Unbalanced Grid Voltage Conditions in Wind Energy Conditions*, IET Renew. Power Gener., **8**, *6*, pp. 687–695 (2014).